

pubs.acs.org/acssensors Article

# Single-Frequency Impedance Studies on an Ionic Liquid-Based Miniaturized Electrochemical Sensor toward Continuous Low-Temperature CO<sub>2</sub> Monitoring

Arun Siddarth Sridhar, Xiaoyu Chen, Tobias Glossmann, Ziming Yang, Yong Xu, Wei Lai, and Xiangqun Zeng\*



Cite This: ACS Sens. 2023, 8, 197-206



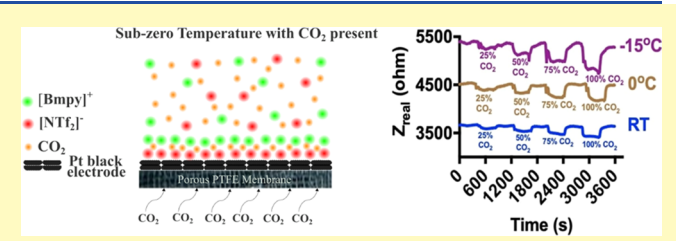
**ACCESS** I

III Metrics & More

Article Recommendations

s Supporting Information

**ABSTRACT:** Continuous greenhouse gas monitoring at sub-zero temperatures is needed for monitoring greenhouse gas emission in cold environments such as the Arctic tundra. This work reports a single-frequency electrochemical impedance sensing (SF-EIS) method for real-time continuous monitoring of carbon dioxide  $(CO_2)$  at a wide range of temperatures (-15 to 40 °C) by using robust ionic liquid (IL) sensing materials and noninvasive, low-power, and low-cost impedance readout mechanisms since they



cause minimal changes in the sensing interface, avoiding the baseline change for long-term continuous sensing. In addition, a miniaturized planar electrochemical sensor was fabricated that incorporates a hydrophobic 1-butyl-1-methylpyrrolidinium bis(trifluromethylsulfonyl)imide ([Bmpy][NTf<sub>2</sub>]) IL electrolyte and Pt black electrode materials. The high viscosity of the ILs facilitates the formation of thin, ordered, and concentrated layers of ionic charges, and the inverse relationship of IL viscosity with temperature makes them especially suited for impedance sensing at low temperatures. The unique low-temperature properties of ILs together with EIS transduction mechanisms are shown to be sensitive and selective for continuously monitoring CO<sub>2</sub> at a –15 to 40 °C temperature range via impedance changes at a specifically selected frequency at the open circuit potential (OCP). Molecular dynamics simulations revealed insights into the structure and dynamics of the IL at varying temperatures in the presence of methane and CO<sub>2</sub> and provided potential explanations for the observed sensing results. The miniaturized and flexible planar electrochemical sensor with the [Bmpy][NTf<sub>2</sub>] electrolyte was tested repeatedly at subzero temperatures over a 58-day period, during which good stability and repeatability were obtained. The CO<sub>2</sub> impedance sensor was further tested for sensing CO<sub>2</sub> from soil samples and shows promising results for their use in real-time monitoring of greenhouse gas emissions in cold temperatures such as permafrost soils.

KEYWORDS: ionic liquid, miniaturized electrochemical sensor, greenhouse gas, carbon dioxide

reenhouse gases (GHG) trap heat and have far-ranging 🔳 environmental and health effects. The increase in global temperatures due to GHG emissions causes the thawing of frozen land such as the Arctic permafrost, resulting in a positive feedback loop of further carbon emissions from build-up organic materials.1-5 It has been predicted that up to 126 billion tons of carbon dioxide (CO<sub>2</sub>) and methane (CH<sub>4</sub>) will be released from permafrost soils by 2100 at the current rate of global warming. The development of accurate, continuous, and in situ methods for measuring GHG concentrations in low-temperature environments is crucial for understanding the effect of global warming on the rate of permafrost carbon release and designing mitigation strategies. Traditional methods of GHG analysis in low-temperature environments such as Arctic soil typically require multiple steps that include sample collection in the fields, transporting frozen samples to laboratories, sample processing, and quantification using analytical tools such as gas chromatography. In addition to being time-consuming, these non-in situ methods are prone to producing inaccurate data resulting from changes in sample

conditions during shipping. They also have more room for human errors in the sampling and sample handling stages. Currently, there are no in situ GHG sensors that can function reliably at extremely cold conditions such as Arctic permafrost, preventing researchers from capturing GHG dynamics at fine scales during the process of permafrost thawing.

Electrochemical transducers are made of compact low-power and low-cost microelectronic circuits that are widely explored for real-time continuous monitoring of chemical species for environmental, health, and domestic and industrial safety applications.<sup>6</sup> However, traditional electrochemical sensors use aqueous media that freezes at subzero temperatures. In recent

Received: September 17, 2022 Accepted: December 21, 2022 Published: January 11, 2023





decades, ionic liquids (IL) containing organic cations or anions have been demonstrated as robust nonvolatile electrolytes and solvents for electrochemical sensors and energy storage devices. Many ILs and/or IL mixtures have freezing points far below 0  $^{\circ}\text{C}$  and are also stable at high temperatures (e.g., >200  $^{\circ}\text{C}$ ). Using ILs as solvents and electrolytes thus eliminates issues experienced with traditional electrochemical sensors (dry-out of solvents and evaporation of electrolytes at high temperatures as well as the freezing of water at low temperatures), making them feasible sensing materials at wide temperature ranges.

The IL-electrode interfacial properties play significant roles in their electrochemical sensing. 111-13 Even though the double layer differential capacitance is a property well defined and characterized for ideally polarizable electrified interfaces for those formed at solid electrodes in contact with aqueous electrolytes, studies of IL-electrode interface properties are much limited, particularly the effect of the temperature on the differential capacitance or impedance at an IL/electrolyte interface with the presence of gaseous solutes.<sup>14</sup> The viscosity of the IL decreases with the increase of temperature. 15 We hypothesize that the high viscosity of ILs at low temperatures will result in the formation of a more dense and concentrated layer of ionic charges on the electrode surface. This relatively rigid IL-electrode double layer at low temperatures can be beneficial for the chemical sensing of gaseous analytes since the molecular interactions between the gas molecules and an IL could result in decreasing resistance by decreasing ionic attractions in the IL. Consequently, the high viscosity of ILs at low temperatures that is usually considered a limitation to practical electrochemical applications in energy storage devices and amperometric sensing (due to the low ionic conductivity of the IL and low diffusion coefficient of the analytes in the IL) becomes an advantage in impedance sensing, since ordered and concentrated electric double layer could provide high sensitivity and selectivity especially at low temperatures. In addition, temperature has an impact on several physicochemical properties of the gaseous analyte in the ILs including viscosity, density, and solubility. For example, the temperaturedependent solubility of gases in the ILs can be utilized to tune selectivity based on the different temperature-dependent solubility equilibrium of the analytes and interferents in the IL.

In this study, taking advantage of the unique physical and chemical properties of ILs with noninvasive low-power and low-cost electrochemical impedance techniques, we developed a novel single-frequency electrochemical impedance sensing (SF-EIS) method for real-time continuous monitoring of CO<sub>2</sub> at low temperatures. In contrast to the widely used electrochemical voltammetric methods that apply a constant or varying DC potential at the working electrode to drive the redox reactions of the analyte for detection, SF-EIS sensing is based on the measurement of the change of interfacial impedance at the electrode-electrolyte interface under an AC perturbation of a few mV amplitudes at a constant frequency that allows real-time, nondestructive chemical sensing. SF-EIS is ideally suitable for long-term and continuous sensing applications due to the minimum perturbation of the sensing interface with low amplitude AC voltage that does not result in interfacial redox reaction(s), thus having minimum change of the sensing interface and minimizing signal baseline drift and with minimum power consumption. CO2 was chosen as the target GHG because CO<sub>2</sub>, along with CH<sub>4</sub>, represents the most important GHG produced in large quantities through

anaerobic respiration and methanogenesis processes in thawing permafrost. 16,17 In addition, we designed and fabricated a miniaturized flexible electrochemical soil gas sensor prototype with Pt black electrodes on a gas-permeable Teflon membrane. Pt black, a fine powder of platinum with good catalytic properties, not only provides a high surface area but also allows simple and robust fabrication of planar electrodes on flexible polymer membranes. Hydrophobic and high-conductivity IL [Bmpy][NTf<sub>2</sub>] was selected as the electrolyte. The functionality of the developed IL-impedance gas sensor was tested for  $CO_2$  sensing over a wide temperature range (-15 to 40 °C). Its application for soil GHG sensing was also tested using natural soil samples. The same sensor device with the ILelectrode interface was tested continuously over short and long periods (i.e., 58 days) to demonstrate its long-term reusability for sensing CO<sub>2</sub> at low temperatures. Our results show that the reported impedance sensor provides the continuous sensing of CO<sub>2</sub> at subzero temperatures. This unique CO<sub>2</sub> sensing method and its sensor prototype when optimized further with enhanced analytical performance and integrated with microsensor electronics is expected to allow in situ monitoring of CO<sub>2</sub> emission in permafrost soils, facilitating the understanding of dynamic changes of soil GHG at various spatial and temporal scales.

#### MATERIALS AND METHODS

Reagents and Materials. 1-Butyl-1-methylpyrrolidinium bis-(trifluromethylsulfonyl)imide ([Bmpy][NTf $_2$ ]) (99%, m.p.  $-18\,^{\circ}$ C) was obtained from Ionic Liquid Technologies GmBH and used as the electrolyte. N $_2$  (Praxair, 99.99%) and instrument-grade CO $_2$  (Praxair, 99.99%) were used as control and the GHG analyte, respectively. Platinum (Pt) black powders were acquired from Sigma-Aldrich (Pt black 205915). Porous polytetrafluoroethylene (PTFE) films were obtained from Interstate Specialty Products (POREX porous PTFE PM6M).

Miniaturized Planar Electrochemical Sensor Fabrication. The miniaturized planar electrochemical sensor device, as shown in Figure 1, is made of three platinum electrodes that were fabricated by

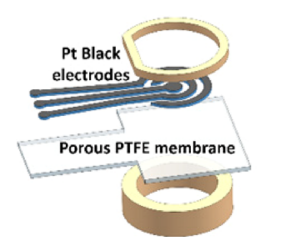




Figure 1. Flexible planar electrochemical soil gas sensor prototype.

evaporating Pt on a porous PTFE film (POREX porous PTFE PM6M) using a polyimide shadow mask. The shadow masks were laser-machined (Epilog Mini 18) out of one millimeter thick and 1 in. wide Kapton tape using 15% speed and 8% power. After the porous PTFE film was attached with the polyimide shadow mask, a 200 nm thick Pt with a 10 nm titanium adhesion layer was deposited by ebeam evaporation (Angstrom Engineering Evaporator). Then, Pt blacks were diluted in deionized (DI) water and evenly pipetted to electrode areas on the PTFE film (defined by the polyimide shadow mask). After the aqueous Pt colloidal suspension dried by natural evaporation at room temperature, another coating was applied. This process was repeated until proper conductivity was achieved. When the DI water evaporates, the Pt black adheres to the evaporated Pt layer most likely by van der Waals force. 18 Afterward, the polyimide shadow mask was peeled off, leaving only patterned metal electrodes on the PTFE film. This facile process does not use any reagents and

thus avoids contamination of the platinum material, which is beneficial for electrochemical sensing. Six sensor devices were made and the details of their uses for different analytical studies in this work are summarized in Table S1. Additional details of fabrication are shown in the Supporting Information.

Testing Set-Up and Sensor Characterization. A packaged electrochemical gas sensor prototype is shown in the left of Figure 1. The working, reference, and counter electrodes made of Pt black are fabricated on a gas-permeable membrane. The top ring, with 19 mm outer diameter, 16 mm inner diameter, and a ~10 mm flat cut edge for folding the PTFE film inside a tube, serves as an electrolyte reservoir and was laser-machined out of a 1.6 mm thick acrylic sheet by 6% speed/12% power. Similarly, the bottom ring, with 19 mm outer diameter and 14 mm inner diameter, functions as a supporting structure and was laser-machined out of a 6 mm thick acrylic sheet by 6% speed/70% power. The [Bmpy][NTf<sub>2</sub>] (100  $\mu$ L) electrolyte was drop-cast onto the three electrode surfaces. The initial device resistance of each fabricated sensor with IL added was measured with a multimeter since it is being used to optimize the sensor fabrication parameters. As shown in the right of Figure 1, the planar and flexible electrode substrate allows easy incorporation into a plastic syringe tube as a soil gas sensor prototype for its insertion into soil for soil GHG sensing applications. Single-frequency electrochemical impedance spectroscopy (SF-EIS) was used as the analytical technique for CO<sub>2</sub> sensor testing at a temperature range from -15 to 40 °C using a Gamry electrochemical workstation. The SF-EIS method uses a sinusoidal AC voltage perturbation with 10 mV amplitude at a constant frequency (e.g., 1 Hz) at open circuit DC potential (i.e., no DC bias potential is applied). The stability of the sensor device was analyzed by repeating SF-EIS experiments for CO2 sensing at 0 °C over multiple days with the same sensor device.

CO<sub>2</sub> Sensing Experiments with Natural Soil Samples. Natural soil samples collected from the Lake Michigan shoreline were used for testing the sensor's capability and sensitivity for measuring soil CO<sub>2</sub>. The properties and chemical composition of the soil have been well characterized and studied<sup>19</sup> (Table S8 in the Supporting Information). To test the sensor for soil gas sensing, the soil samples were conditioned with a controlled amount of CO<sub>2</sub> gas by purging the soil with CO<sub>2</sub> at a flow rate of 500 sccm for 1 h. After equilibrating, the release of CO<sub>2</sub> from this soil sample was immediately measured using our sensor device and SF-EIS methods. All single-frequency experiments were conducted at open circuit DC potential with a sinusoidal AC voltage at a 10 mV amplitude at 1 Hz.

Computational Methods. Molecular dynamics (MD) simulations were used to investigate the conductivity and structure of the IL electrolyte with and without the presence of the gaseous analytes at low and high temperatures. Coherent conductivity can be calculated using statistical mechanics methods based on the fluctuation—dissipation theorem. We track the center of mass velocity changes of all molecules of each type together weighted with their charge to capture coherent conductivity. We used a model of 240 ion pairs (Table S7) with periodic boundary conditions to determine the coherent conductivity and throughout 6 ns of simulated real-time. Detailed computation methods are in the Supporting Information.

#### ■ RESULTS AND DISCUSSION

SF-EIS Method for Real-Time and Continuous Sensing. For real-time and continuous sensing of an analyte, SF-EIS is the most suitable readout method that measures the changes in electrochemical impedance upon exposure to the analyte versus time at a selected constant frequency under a sinusoidal AC voltage perturbation with small amplitude (e.g., 10 mV). The typical single-frequency impedance measurement is made with a constant DC potential applied to the working electrode of the electrochemical system. However, hysteresis effects in potential-dependent double layer capacitance of ILs at both the Pt electrode and Au electrode were reported. The slow pseudocapacitive processes are particularly apparent

at a frequency below 10 Hz and this hysteresis of the IL–electrode interface has been interpreted as the slow relaxation of the electric double layer structure when a DC potential was applied to the electrode. Thus, the hysteresis effect can lead to the slow drift of the baseline signal when a DC potential is applied. To address this issue, a smaller DC bias potential of –0.3 V or zero volts is used in our early work. <sup>24,25</sup> Here, we set the electrode potential at an open circuit potential, i.e., no DC potential is applied to our electrochemical sensor system in our SF-EIS experiments to prevent the hysteresis effect at the IL/electrode interface. This also minimizes the power consumption for long-term continuous gas sensing in the field.

In the SF-EIS method, the impedance was measured between the working and reference electrodes. As shown in Figure S1, the Nyquist plot in which the impedance response of the full frequency range (100 kHz to 0.1 Hz) at room temperature without CO2 is shown. The impedance response at the low-frequency range can be modeled by the standard Randles equivalent circuit with electrolyte resistance  $R_{\rm e}$ , charge-transfer resistance  $R_{ct}$ , double-layer capacitance  $C_{dl}$ , and diffusion element W, as shown in the Figure S1 inset. Figure S2 summarizes the linear plots of  $Z_{real}$  values vs  $CO_2$ concentrations measured at constant frequencies of 0.1, 1, and 10 Hz. The slopes of these plots were used to determine the sensor sensitivity to CO<sub>2</sub> concentration at these frequencies. The sensitivity increases with decreasing frequency with 0.1 Hz (-8.642 Ohm/% CO<sub>2</sub>) being the highest, followed by 1 Hz  $(-3.916 \text{ Ohm/}\% \text{ CO}_2)$  and 10 Hz  $(-3.844 \text{ Ohm/}\% \text{ CO}_2)$ . To compare the signal-to-noise ratio, the average impedance at each CO<sub>2</sub> concentration was calculated by averaging the CO<sub>2</sub> impedance data points at each concentration and we calculated the relative standard deviation in the nitrogen background. The baseline relative standard deviation of the nitrogen background was 0.42% at 0.1 Hz that is higher than that at 1 Hz (0.31%). This indicates that although the sensitivity was higher at 0.1 Hz compared to 1 Hz, the noise was also more significant at higher frequencies so the signal/noise ratio is not improved significantly at low frequencies. Higher frequencies also allow fast data acquisition, which is preferred for real-time in situ gas monitoring. The average time to obtain a data point at 0.1 Hz is significantly slower than at 1 Hz. Considering these factors, 1 Hz was chosen as an optimal frequency for our SF-EIS experiments.

Temperature Dependence of CO<sub>2</sub> Impedance Sensor Sensitivity with the SF-EIS Method. The sensitivity of the miniaturized CO2 sensor was studied by conducting SF-EIS experiments at different temperatures from −15 to 40 °C, and 1 Hz was chosen as the AC frequency. The sub-zero temperatures tested have been reported to be representative of permafrost soils.<sup>26</sup> Figure 2a shows the SF-EIS results at different temperatures when the sensor is exposed over time to a series of controlled CO<sub>2</sub> concentrations (0-100%), with periods of zero concentration in between each controlled analyte concentration. A decrease in  $Z_{\text{real}}$  with an increase in CO<sub>2</sub> concentration can be observed (Figure 2b). Sensor sensitivity and repeatability at different temperatures can be determined from the calibration curve of the sensor obtained from the recorded data. As shown in Figure 2a and summarized in Table S2, the slope of the calibration curve (i.e., sensitivity) of the IL impedance sensor to CO2 concentration is generally higher at sub-zero temperatures when compared to those at room temperature and 40 °C. In

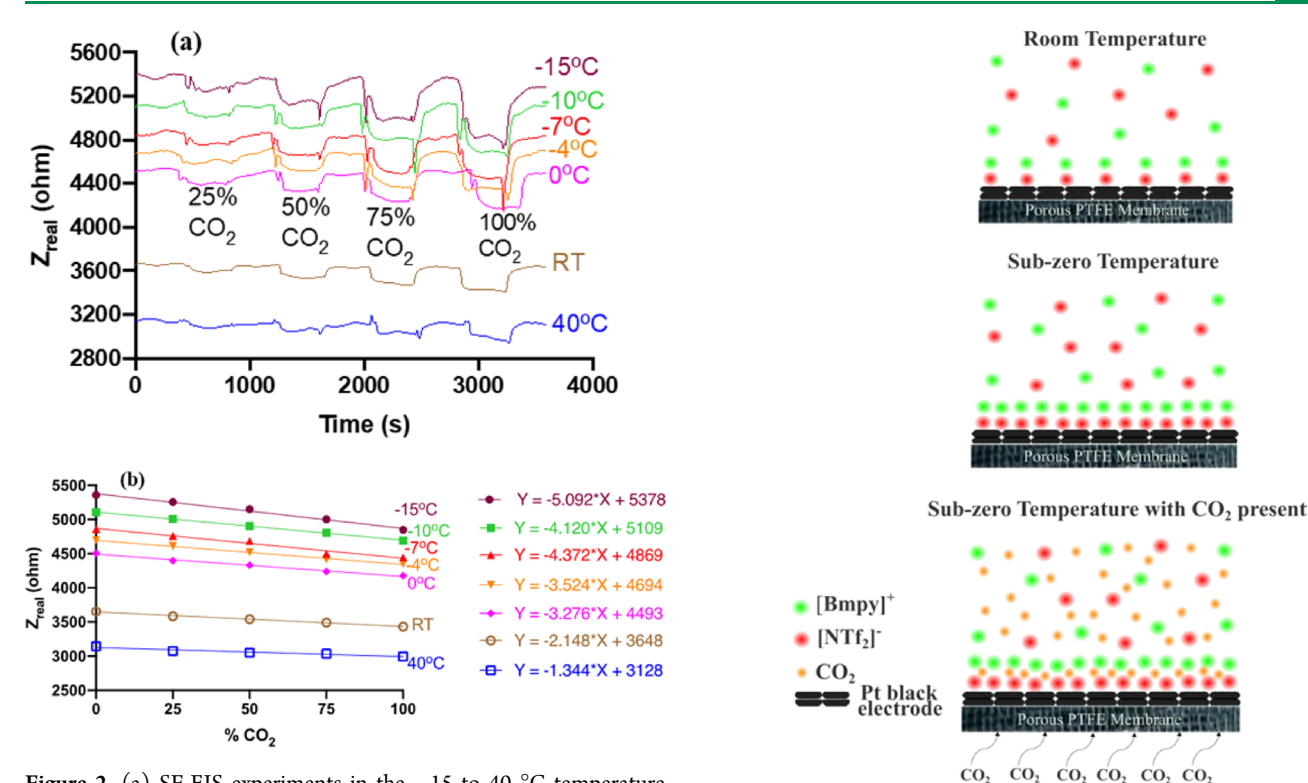


**Figure 2.** (a) SF-EIS experiments in the -15 to 40 °C temperature range; (b) linear calibration curves. Frequency: 1 Hz, AC voltage: 10 mV, DC bias: OCP. Same sensor device was used in all these experiments carried out on two consecutive days, i.e., 40 °C, RT, -10 and -15 °C tested on day one and 0, -4 and -7 °C tested in the following day.

addition, the initial impedance (i.e.,  $Z_{\text{real(i)}}$  at 0% CO<sub>2</sub>) is increased with decreasing temperature.

The results of the initial impedance at varying temperatures shown in Figure 2 are consistent with Walden's rule of the temperature-dependent conductivity-viscosity relationship of liquids. The viscosities  $(\eta)$  of many ILs were well characterized. Generally, the viscosity of ILs increases with decreasing temperatures; in other words, its fluidity  $(\eta^{-1})$ increases as the temperature increases. 15 Thus, a more densely packed layer of ionic charges at the IL-electrode interface is expected at low temperatures, as shown in Figure 3. Based on the Walden relationship of the conductivity vs viscosity of liquid electrolytes, the absolute impedance of the IL-electrode interface (defined here as initial impedance  $(Z_{real})$ ) should increase with decreasing temperature. Our results shown in Table S2b and Figure 2 are consistent with this trend. Densities of ILs are shown to decrease with the increase of temperature, following a quadratic polynomial relationship. 15 Since ILs have significantly higher ionic densities at lower temperatures, our results can also be interpreted as a density effect. While the viscosity and density of the IL increase with decreasing temperatures, there is also a competing effect of CO<sub>2</sub> solvation, as the solubility of CO<sub>2</sub> is expected to be higher at lower temperatures, e.g., in imidazolium-based ILs.<sup>2</sup> Additional studies of CO2 solubility in ILs at various temperatures were also reported but with inconsistent observations. 11,12 Our experimental results in Figure 2 suggest that the influence of viscosity and density dominates over that of solubility, leading to increased impedance despite higher CO<sub>2</sub> concentration at lower temperatures. Early work shows that the anion of the IL dominates the interactions with CO<sub>2</sub>,

Figure 3. Schematics of changes of IL—electrode interfacial properties for impedance-based  $\rm CO_2$  sensing at different temperatures.

with the cation playing a secondary role. As a result, the decrease of the impedance in the presence of the  $CO_2$  solute is likely the results of  $CO_2$  interactions with  $NTf_2$  anion that decreases the ion attraction between the cation and anion of the IL.

CO<sub>2</sub> adsorption into the IL/electrode interface could affect the IL/electrode interface capacitance. Early observation shows that differential capacitance increased with an increasing temperature between 80 and 140 °C.<sup>11</sup> Other computer simulation studies at a wide temperature and density range based on the restricted primitive model of an electrolyte near a charged hard wall showed that the capacitance of the interface is quantitatively similar between the high- and low-density regimes. In both cases, the capacitance has a negative slope at high temperatures and a positive slope at low temperatures. Therefore, these results imply that the behavior of the capacitance at low temperatures is not a density but a temperature effect, because the properties of the IL-electrode interface are temperature-dependent. However, these prior studies did not consider subzero temperatures. The capacitance changes due to the interaction of CO2 and anions or cations in the double layer are expected to be more complex. Thus, in this work, we used impedance as the sensing signal rather than capacitance sensing based on the effects of CO<sub>2</sub> adsorption into the IL/electrode interface.

MD Study of IL/Electrode Interface Structures and Properties at Varying Temperatures. To further understand the molecular mechanism of the interface impedance change with or without gaseous solutes at various temperatures, we applied MD simulations to investigate the conductivity of the IL solutions and their structure at various temperature conditions. Coherent conductivity as measured in SF-EIS experiments can be calculated using statistical

mechanics methods that are based on the fluctuation—dissipation theorem. <sup>28</sup> ILs made of large and bulky charged ions with permanent dipole moments interact with each other via directional electrostatic interactions. The interactions of the solute with the cation or anion of ILs via electrostatic or van der Waals interactions could lead to changes in conductivity, e.g., weakening the cation-anion interactions to increase the ionic conductivity, strengthening the interactions to decrease the conductivity, or insignificant change of the interactions leading to negligible changes in conductivity. Research shows that the ions often self-assemble into well-defined nanostructures in the bulk. 11-13 Bulk ILs often have a spongelike nanostructure due to the segregation of charged and uncharged groups into separate domains. CO2 and CH4 are both nonpolar molecules since the individual bond dipoles cancel each other which results in zero net dipole moment. Recent work shows a strong correlation between the ratio of unoccupied space in pure ILs and their ability to absorb CO<sub>2</sub>. <sup>29</sup> Our selection of the hydrophobic [Bmpy][NTf2] as our electrolyte provides a high amount of unoccupied spaces due to the bulky Bmpy cations. The hydrophobic NTf2 anion is shown to weaken cationanion interactions, enabling higher absorptivity of CO<sub>2</sub>. Water-anion attraction is relatively weak in ILs with smaller anions, likely due to a more distributed charge in NTf<sub>2</sub>, impeding the absorption of H<sub>2</sub>O and minimizing the interference from humidity at ambient conditions.<sup>29</sup> Our MD simulation with 240 ion pairs confirms that even at a very high concentration of CO<sub>2</sub> or methane dissolved in the IL, it only leads to a small increase of the size of our periodic simulation cell. As shown in Table S7, the addition of gaseous molecules CO2 and CH4 leads to less volume increase at lower temperatures.

As shown in Figure 4, our computational study shows a surprising trend. The conductivity increases with the addition

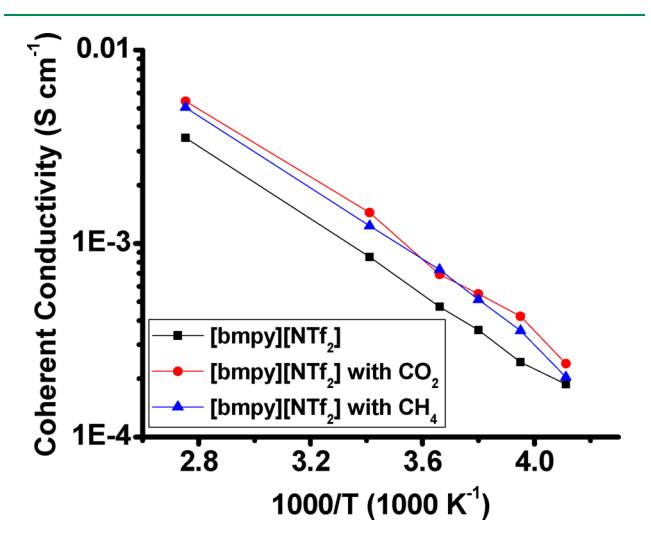


**Figure 4.** Coherent conductivity of [Bmpy][NTf<sub>2</sub>] solutions obtained by MD simulation.

of CO<sub>2</sub> and CH<sub>4</sub>, but at lower temperatures, CH<sub>4</sub> does not increase the conductivity at all. The discovered phenomenon should not be interpreted as an absolute correlation to simulate temperature conditions, given the limitations of MD with regard to conductivity, especially for ILs due to the trading of complexity for significantly lower computation cost. Structure considerations help explain this result. We calculated radial

distribution functions (RDFs) of all atom force field types. We need to understand why the conductivity is increased by CO<sub>2</sub> but not as much or even not at all by CH<sub>4</sub> at low temperatures. RDFs in Figure 5 show some differences between CH<sub>4</sub>/IL in

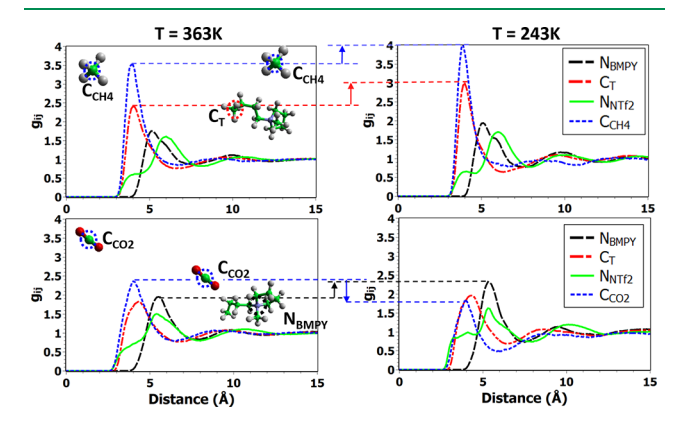


**Figure 5.** RDFs (probability density) relative to the carbon center of the relevant analyte.

the upper part of the figure and the CO<sub>2</sub>/IL in the lower part as well as the temperature evolution. CH<sub>4</sub> can be found more frequently near C<sub>T</sub>, which is the force field name of the terminal carbon of the alkyl tail of the cation of the IL. Interestingly, at lower temperatures, the probability increases even more. We note further that CH<sub>4</sub> can be found more frequently near another methane molecule. CO<sub>2</sub> molecules are clearly better dispersed in the IL. For CO2, we notice a very different trend, namely, a better dispersion in the IL at low temperatures, which could mean better solubility as well. CO2 is slightly more likely found near the NTf2 anion at low temperatures (Figure 5, green solid line). The absolute distance from any analyte molecule of course has to be understood in the context of the structures involved. For example, the CH<sub>4</sub> carbon will always have a distance greater than about 4 Å to a terminal alkyl carbon in Bmpy<sup>+</sup> simply because hydrogen atoms sterically separate these carbons. Names for atomic species for the used molecules are illustrated for clarity in Figure 5.

As Shimizu et al. pointed out previously, long alkyl chain cations in the ILs tend to form nonpolar domains. We confirmed the presence of such domains via the RDF, as shown in Figure 6. A distance of four Angstroms is roughly

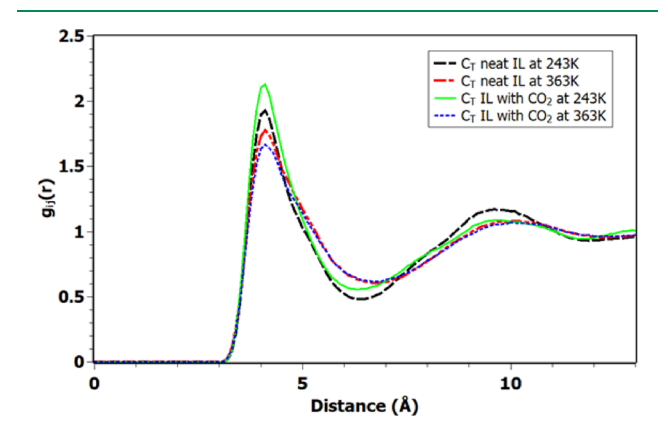


**Figure 6.** RDF of the terminal carbon of the cation alkyl chain to the same carbon in other [Bmpy] cations.

how close two terminal carbons can be. The probability density peaks exactly at that distance. At lower temperatures, this trend is stronger (black dashed line) but the addition of analyte (either CO<sub>2</sub> or CH<sub>4</sub>) enhances this effect even more, however, only at 243 K and not at 263 K. Given the presence of nonpolar domains and the earlier finding of the strong coordination of methane to the alkyl end of the cation of the IL, the reason for CH<sub>4</sub> impacting the conductivity of the solution less, especially at low temperatures is found. Cationanion interactions are disrupted more by the addition of CO2 than CH<sub>4</sub> as the alkyl end holds less charge density and methane can even accumulate in these areas. The ring-end of the cation of the IL will pair up with the anion as if no methane was added; at least, we expect that to happen to a certain concentration. Even though the full effect of CH<sub>4</sub> no longer increasing conductivity is evident at around -30 °C, the trend shown in Figure 4 and analyzed RDFs in Figures 5 and 6 provide more confidence that the predicted ordering could very well occur at higher temperatures such as -10 °C. MD only gives us the trend that needs to be further validated by experimental data.<sup>30</sup>

Repeatability and Stability of the IL CO<sub>2</sub> Impedance Sensor. For continuous GHG monitoring at low temperature environments, it is crucial to test sensors over both short and longer periods of time in order to understand the effect of external conditions on sensor performance. This would enable the development of methods for efficient calibration and device maintenance. The short-term repeatability of the sensing signal was measured by conducting SF-EIS sensing using the same sensor device by alternating the gas sample either with N<sub>2</sub> gas or 50% CO<sub>2</sub> at 400 s intervals for three cycles. The relative standard deviations of  $Z_{\text{real}}$  values between three averages in the presence of an analyte at different temperatures were calculated and are shown in Figure S6. It can be seen that the relative standard deviation values are relatively small (less than 0.25%), indicating the repeatability of CO<sub>2</sub> sensing signals. In addition, there is no particular relationship between standard deviation values and temperature. In order to study the stability of the miniaturized gas sensor over longer time periods, SF-EIS experiments were conducted using the same sensor device over a 58-day period that is stored in ambient conditions when it was not under test. These conditions were chosen to mimic the practical usage of the sensor for continuous CO2 sensing in low temperature environments. Figure 7a shows the  $Z_{real}$  values recorded at 50% CO<sub>2</sub> in a N<sub>2</sub> background over a period of days. Two observations can be seen from these data: (1) At each test, the impedance  $Z_{\text{real}}$ decreases in the presence of CO<sub>2</sub> compared to the background signal; (2) The initial impedance  $Z_{\text{real}}$  values of the sensor in both CO<sub>2</sub> and N<sub>2</sub> backgrounds remain consistent within a few days of the test but they shifted after a long storage time (e.g., weeks). The shifts of the initial impedance value of the sensor measured in N2 conditions reflect the impacts of environmental conditions on its properties due to its storage at ambient conditions.

We hypothesize that this shift in initial impedance measured in  $N_2$  conditions after the sensor is stored in the ambient conditions is a result of the Pt black electrode being partially oxidized over longer periods of storage at ambient conditions. All single-frequency experiments to measure  $Z_{\text{real}}$  values in the presence of  $N_2$  and  $CO_2$  were conducted at open circuit potential (OCP). Figure S7 summarizes the average OCP of the sensor device during the multiple-day experiments that

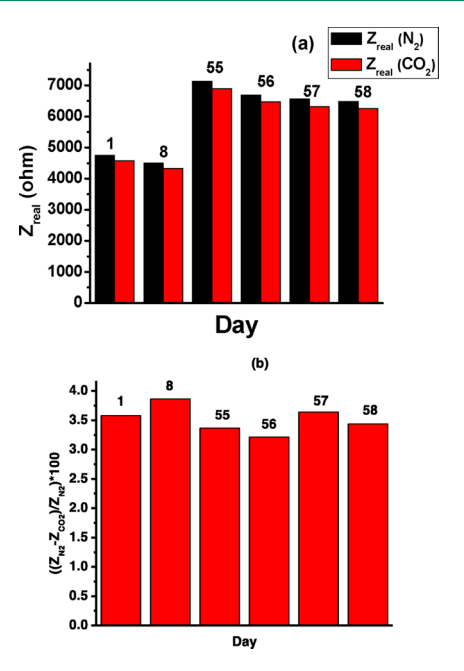


Figure 7. (a) Comparison of multiday average sensor signal  $Z_{\rm real}$  with the same sensor under background conditions: N<sub>2</sub> and 50% CO<sub>2</sub>; (b) relative  $Z_{\rm real}$  change vs days. Experimental conditions: same sensor device; temperature at 0 °C, AC frequency: 1 Hz, 10 mV AC, DC potential is set at OCP.

show about 80 mV change of OCP values. The OCP of platinum electrodes in oxygenated systems has been studied previously and reported<sup>31</sup> in the presence of oxygen, and OCP is generally considered to be at a mixed potential, with the reduction of oxygen being the predominant cathodic process and platinum oxide formation being the predominant anodic process. Previous studies<sup>31</sup> have shown that when oxygen is absent, the Pt electrode rests at more negative potentials. This is because when there is no oxygen present, there is no cathodic current from oxygen reduction and the electrode rests at a more negative potential to offset the anodic current from the oxidation of trace impurities<sup>32</sup> and Pt dissolution. When oxygen is present, PtO<sub>x</sub> formation occurs and the oxygen reduction reaction proceeds at faster rates on oxygen-covered sites than on bare sites due to the relative strengths of the platinum-oxygen and platinum oxide-oxygen bonds.<sup>33</sup> The anodized nature of the local Pt/PtO<sub>x</sub> reaction results in more PtO<sub>x</sub> accumulation on the surface, which in turn provides more sites on which the oxygen reduction reaction will occur. Eventually, the anodic PtO<sub>x</sub> formation reaction has been shown<sup>33</sup> to proceed with increased current density and polarization, leading to more positive rest potentials and predominant surface coverage of PtO<sub>x</sub>. However, over longer periods of time, the cathodic reduction reaction of PtO<sub>x</sub> recovers some Pt sites, resulting in fluctuating mixed potential which is still more positive compared to the resting potential in the absence of oxygen.<sup>33</sup> The nature of PtO<sub>x</sub> coverage also affects conductance in relation to bare Pt, as shown in previous studies.34

We carried OCP measurements on a miniaturized sensor device using controlled concentrations of oxygen over a three-week period and the same sensor device was used in this study. In the first week, oxygen concentrations from 0–7% diluted in nitrogen carrier gas were introduced into a freshly made miniaturized sensor device and the average OCP over a 10-min

period was recorded for each oxygen concentration. This was followed by OCP measurements in nitrogen-diluted air (14 to 25%  $\rm O_2$  concentration) in the second week and OCP measurements in 1–25% oxygen concentrations diluted with nitrogen gas in the third week using the same sensor device. Figure 8 shows the plots of OCP vs oxygen concentration in

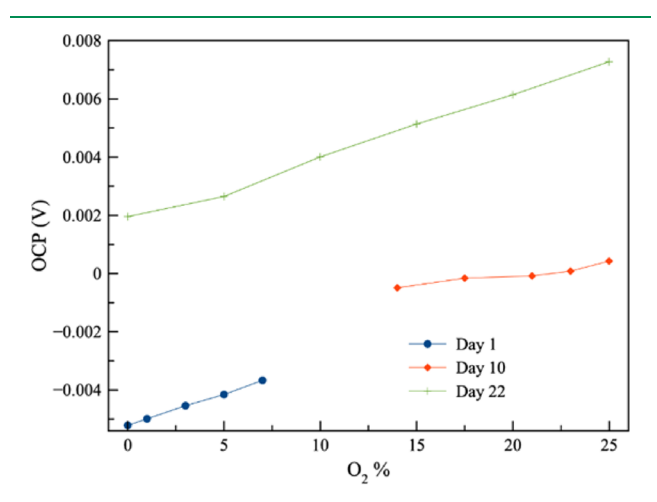


Figure 8. OCP-time plots at different concentrations of oxygen over three weeks, 10-min average reported for each measurement. Experimental conditions: sensor O, temperature: 0  $^{\circ}$ C, background gas: N<sub>2</sub> (Day 1), air (Day 10), N<sub>2</sub> (Day 22).

these three weekly measurements. In all three measurements, it can be seen that the OCP shifts positively with the overall oxygen concentration, consistent with previous rest potential data in the presence and absence of oxygen. It was also seen that the overall OCP increases with time in the initial three weeks of measurement, likely as a result of  $\text{PtO}_x$  accumulation on the electrode surface.

A practical sensor for real-world applications would be placed under ambient conditions where differing amounts of oxygen could be present in the sensor environment over longterm usage. The signal-to-noise ratio limits the resolution of every sensor. Our test results show that the relative change in the impedance signal in the presence of the same concentration of CO2 is the same during repeated tests in N<sub>2</sub> background gas. As shown in Figure 7b, the relative change of the impedance signal  $(Z_{N2} - Z_{CO2}/Z_{N2})$  over multiple days for the same CO<sub>2</sub> concentration is less than 5%. Experiments using air as the background gas also show that the differential impedance ( $dZ_{real}$ ) in the presence of  $CO_2$  is consistent over three cycles (Figure S10). Since the shift in the background impedance signal does not affect the overall sensing performance, sensor packaging and calibration methods can be developed to mitigate this baseline signal change for longterm sensing applications.

Selectivity of IL CO<sub>2</sub> Impedance Sensors in the Presence of Methane. To demonstrate the selectivity of our sensor in air/oxygen environments, we conducted the same single-frequency experiments in an air background instead of nitrogen. These experiments were conducted using sensor S, which was previously used for experiments in natural soil samples. This sensor is over 2 years old, and it was stored in ambient conditions. No fresh IL was added prior to these new experiments in the air background. As seen from Figure S10, reproducible signals at 10% CO<sub>2</sub> concentration are seen at both room temperature and 0 °C. The increased background

drift and noise are likely a result of sensor aging. However, the impedance change  $(dZ_{real})$  in the presence of  $CO_2$  is consistent over three cycles (where  $dZ_{real} = Z_{real}$  (N<sub>2</sub> average) -  $Z_{real}$ (CO<sub>2</sub> average)). This shows that our sensor is selective to CO<sub>2</sub> in the presence of oxygen/air and is capable of producing stable CO<sub>2</sub> signals even after long-term storage. In addition to CO<sub>2</sub>, CH<sub>4</sub> is another major GHG in permafrost soils, which is produced by methanogenesis in anaerobic soil environments. In order to study the selectivity of the miniaturized sensor for CO<sub>2</sub> detection in the presence of CH<sub>4</sub>, SF-EIS experiments in the presence of CH<sub>4</sub> were conducted under similar conditions to that of  $CO_2$ . In these experiments, the  $Z_{real}$  values were continuously recorded over a 10-min period in the presence of N<sub>2</sub> (control), 50% CO<sub>2</sub>, and 50% CH<sub>4</sub> at room temperature and different subzero temperatures. Relatively high concentrations of these gases were chosen for this selectivity test to highlight their effects on the IL impedance gas sensor. Figure 9a provides the histogram of average  $Z_{\text{real}}$  values for CO<sub>2</sub>, CH<sub>4</sub>,

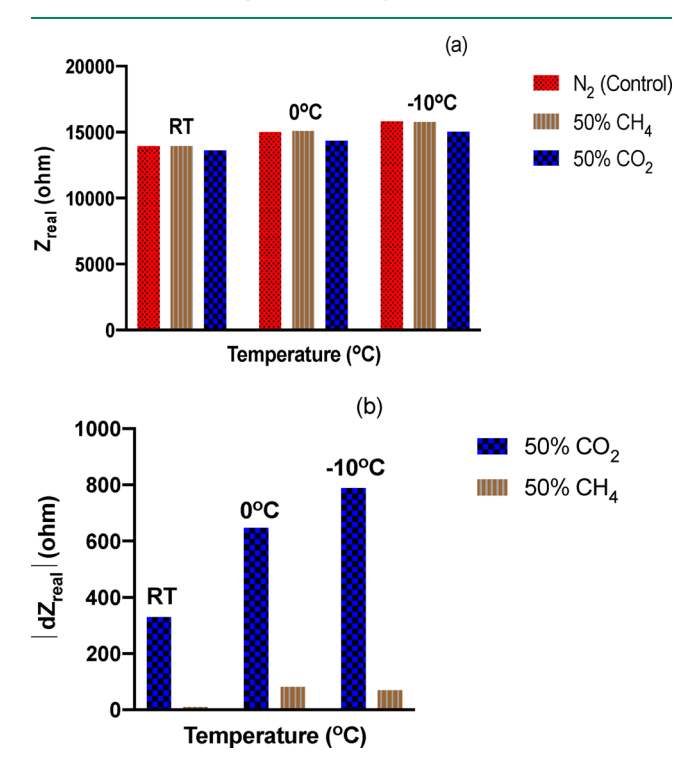


**Figure 9.** Selectivity experiments in the presence of methane: (a) average  $Z_{\rm real}$  values in the  $N_2$  background, 50% CO $_2$ , and 50% CH $_4$  respectively, (b) absolute  $dZ_{\rm real}$  values, where  $dZ_{\rm real} = Z_{\rm real}$  ( $N_2$  control)  $-Z_{\rm real}$  (analyte gas). DC potential: OCP, AC bias: 10 mV, frequency: 1 Hz, sensor device: "SE".

and  $N_2$  at different temperatures. It can be seen from Figure 9 that the average  $Z_{\rm real}$  values decrease significantly when  $CO_2$  is introduced to the sensor, whereas the  $Z_{\rm real}$  signal in the presence of  $CH_4$  is similar to that of background  $N_2$  control. This is further visualized in Figure 9b, which compares the difference in  $Z_{\rm real}$  between  $N_2$ ,  $CO_2$ , or  $CH_4$  analyte gas  $(dZ_{\rm real})$  at different temperatures. Hence, our data indicate that the sensor is selective for  $CO_2$  detection in the presence of  $CH_4$ , and thus, it can be used to separately quantify  $CO_2$  in soil environments where  $CH_4$  would also be present.

CO<sub>2</sub> Sensing in Natural Soil Samples. The collected natural soil samples (see the Materials and Methods Section) were used for preliminary soil gas sensing experiments using

the CO<sub>2</sub> impedance sensor tested above. In these experiments, the sensor was placed on the soil surface, and SF-EIS experiments were conducted using the same sensor device at 40 °C (first day), -4, -7, and -10 °C (second day), and 0 °C (third day) to measure the CO<sub>2</sub> concentrations released from the soils with different initial CO<sub>2</sub> concentrations. Since all the sensor tests were performed with one sensor device, these experiments at different temperatures were carried out on different days. Note that the control experiments in N2 background gas and in the soil sample doped with CO2 at each temperature were performed on the same day. In addition, the increasing impedance trend with decreasing temperature is the same for each individual day's measurements and is consistent. The comparative raw data for these experiments are shown in Figure S9a-f. At each temperature, it can be seen that the  $Z_{\rm real}$  values measured from SF-EIS experiments decreased significantly when the sensor was placed in soil samples that were prepurged with CO<sub>2</sub> for 1 h. As discussed above, this decrease in resistive impedance  $Z_{\rm real}$ could be attributed to molecular interactions between the CO<sub>2</sub> analyte and [Bmpy][NTf2] IL that result in decreasing resistance and increasing conductivity by decreasing ionic attractions in the IL. Our current experiments show that the background signal drift direction is opposite to the direction of signal change in the presence of CO<sub>2</sub>, these data show that our sensor is sensitive to soil CO<sub>2</sub> emission even in the presence of the signal drifts. Figure 10 provides the comparative histo-

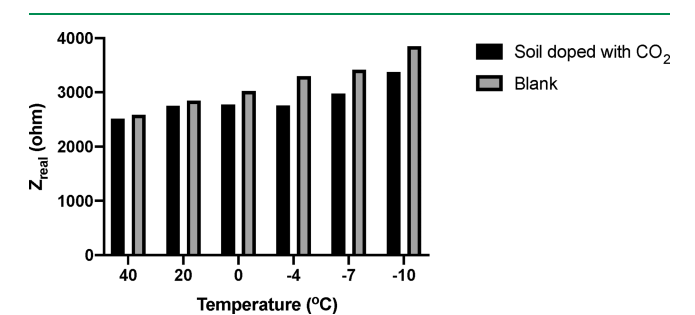


Figure 10. Summary of control and  $CO_2$   $Z_{real}$  values in soil sample tests, gray color: blank soil sample, black color: soil sample purged with  $CO_2$  for an hour.

grams of average  $Z_{\rm real}$  values of the sensor obtained when measuring the same soil samples with and without  ${\rm CO_2}$  purging. In both the control and  ${\rm CO_2}$  purging experiments, the average  $Z_{\rm real}$  increases with decreasing temperature due to the increased viscosity of the IL electrolyte with decreased temperature. In addition, the sensitivity for  ${\rm CO_2}$  detection increases with decreasing temperature. These soil sensing data are consistent with our previous  ${\rm CO_2}$  sensing experimental results, indicating the effectiveness of our method for  ${\rm CO_2}$  detection in real soil samples at low temperature conditions.

#### CONCLUSIONS

Real-time and continuous-use gas sensors are needed for environmental monitoring of GHS emissions in a cold environment. In this work, we conducted temperature-dependent studies with both computational and experimental approaches on a novel IL-based single-frequency impedance sensor for continuously monitoring  $CO_2$  gas from subzero to ambient temperatures using IL [Bmpy][NTf<sub>2</sub>] as the electrolyte with miniaturized planar Pt black electrodes in the absence

of DC potential applied. The real impedance  $(Z_{real})$  is shown to decrease linearly with an increase in %CO2, which could be attributed to molecular interactions between the CO2 analyte and IL [Bmpy][NTf<sub>2</sub>] that result in decreasing resistance and increasing conductivity due to decreased ionic attractions in the IL. The increased viscosity of the IL at lower temperatures resulted in the formation of more concentrated layers of ionic charges and proved to be beneficial for sensitivity enhancement for our impedance-based gas sensing method. The sensor device with the IL electrolyte shows good stability at ambient conditions. Continuous sensing experiments conducted with the same miniaturized planar sensor device over a 58-day period of time showed that no dry-out and freeze of the IL electrolytes occurred. Changes in background signals during these continuous sensing experiments over the 58-day period were explained based on the change of OCP of the sensor device at ambient conditions due to partial oxidation of Pt black electrode materials. However, our results show that Pt electrode changes did not affect the net relative CO2 signal using either N2 or air as background gas. Since ILs have the durability of traditional inorganic materials (e.g., metal oxides) and the tunability and synthetic flexibility of the organic materials, the noninvasive impedance sensing together with the unique properties of ILs minimizes the fouling or poisoning of the electrode and electrolyte compared to those amperometric sensors based on redox reactions. To our knowledge, this is the first report on low-temperature impedance sensing. Our sensing method that works at cold temperatures would be suitable for permafrost soil measurements. Our future work includes field testing the sensors in Arctic soils, optimizing sensor performance by increasing the signal/noise ratio, and designing better IL/electrode interfaces such as using optimal nanoelectrode materials, IL electrolytes, and sensor fabrication and packaging. We also aim to enhance the sensor sensitivity and selectivity for continuous soil CO2 monitoring under realworld conditions.

#### ASSOCIATED CONTENT

#### **5** Supporting Information

The Supporting Information is available free of charge at https://pubs.acs.org/doi/10.1021/acssensors.2c02040.

Additional details on experimental conditions; computational methods and more data on soil testing; repeatability; and effect of frequency/device resistance (PDF)

#### AUTHOR INFORMATION

#### Corresponding Author

Xiangqun Zeng — Department of Chemistry, Oakland University, Rochester Hills, Michigan 48309, United States; Email: zeng@oakland.edu

#### Authors

Arun Siddarth Sridhar — Department of Chemistry, Oakland University, Rochester Hills, Michigan 48309, United States; orcid.org/0000-0002-1288-577X

Xiaoyu Chen — Department of Electrical and Computer Engineering, Wayne State University, Detroit, Michigan 48202, United States

Tobias Glossmann — Department of Chemistry, Oakland University, Rochester Hills, Michigan 48309, United States; orcid.org/0000-0002-2857-0211

- Ziming Yang Department of Chemistry, Oakland University, Rochester Hills, Michigan 48309, United States;
  ocid.org/0000-0003-0312-8408
- Yong Xu Department of Electrical and Computer Engineering, Wayne State University, Detroit, Michigan 48202, United States; ⊙ orcid.org/0000-0003-4440-7980
- Wei Lai Department of Chemical Engineering and Materials Science, Michigan State University, East Lansing, Michigan 48824, United States; orcid.org/0000-0002-9258-5573

Complete contact information is available at: https://pubs.acs.org/10.1021/acssensors.2c02040

#### **Author Contributions**

The manuscript was written through the contributions of all authors.

#### **Notes**

The authors declare no competing financial interest.

#### ACKNOWLEDGMENTS

We thank the support from the U.S. National Science Foundation (NSF) under Grant CBET-1841301 and 2034323.

#### REFERENCES

- (1) Schuur, E. A. G.; McGuire, A. D.; Schädel, C.; Grosse, G.; Harden, J. W.; Hayes, D. J.; Hugelius, G.; Koven, C. D.; Kuhry, P.; Lawrence, D. M.; Natali, S. M.; Olefeldt, D.; Romanovsky, V. E.; Schaefer, K.; Turetsky, M. R.; Treat, C. C.; Vonk, J. E. Climate Change and the Permafrost Carbon Feedback. *Nature* **2015**, *520*, 171–179.
- (2) McCalley, C. K.; Woodcroft, B. J.; Hodgkins, S. B.; Wehr, R. A.; Kim, E.-H.; Mondav, R.; Crill, P. M.; Chanton, J. P.; Rich, V. I.; Tyson, G. W.; Saleska, S. R. Methane Dynamics Regulated by Microbial Community Response to Permafrost Thaw. *Nature* **2014**, *514*, 478–481.
- (3) Tveit, A. T.; Urich, T.; Frenzel, P.; Svenning, M. M. Metabolic and Trophic Interactions Modulate Methane Production by Arctic Peat Microbiota in Response to Warming. *Proc. Natl. Acad. Sci. U. S. A.* 2015, *112*, E2507–E2516.
- (4) Blaud, A.; Lerch, T. Z.; Phoenix, G. K.; Osborn, A. M. Arctic Soil Microbial Diversity in a Changing World. *Res. Microbiol.* **2015**, *166*, 796–813.
- (5) Euskirchen, E. S.; Bret-Harte, M. S.; Shaver, G. R.; Edgar, C. W.; Romanovsky, V. E. Long-Term Release of Carbon Dioxide from Arctic Tundra Ecosystems in Alaska. *Ecosystems* **2017**, *20*, 960–974.
- (6) Rehman, A.; Zeng, X. Methods and Approaches of Utilizing Ionic Liquids as Gas Sensing Materials. *RSC Adv.* **2015**, *5*, 58371–58392.
- (7) Fujie, K.; Otsubo, K.; Ikeda, R.; Yamada, T.; Kitagawa, H. Low Temperature Ionic Conductor: Ionic Liquid Incorporated within a Metal—Organic Framework. *Chem. Sci.* **2015**, *6*, 4306–4310.
- (8) Lazzus, J. A. A Group Contribution Method for Predicting the Freezing Point of Ionic Liquids. *Period. Polytech. Chem. Eng.* **2016**, *60*, 273–281.
- (9) Vogl, T.; Passerini, S.; Balducci, A. The Impact of Mixtures of Protic Ionic Liquids on the Operative Temperature Range of Use of Battery Systems. *Electrochem. Commun.* **2017**, *78*, 47–50.
- (10) Kunze, M.; Jeong, S.; Appetecchi, G. B.; Schönhoff, M.; Winter, M.; Passerini, S. Mixtures of Ionic Liquids for Low Temperature Electrolytes. *Electrochim. Acta* **2012**, *82*, 69–74.
- (11) Lockett, V.; Sedev, R.; Ralston, J.; Horne, M.; Rodopoulos, T. Differential Capacitance of the Electrical Double Layer in Imidazolium-Based Ionic Liquids: Influence of Potential, Cation Size, and Temperature. *J. Phys. Chem. C* **2008**, *112*, 7486–7495.
- (12) Pizio, O.; Sokołowski, S.; Sokołowska, Z. Electric Double Layer Capacitance of Restricted Primitive Model for an Ionic Fluid in Slit-

- like Nanopores: A Density Functional Approach. J. Chem. Phys. 2012, 137, 234705.
- (13) Holovko, M.; Kapko, V.; Henderson, D.; Boda, D. On the Influence of Ionic Association on the Capacitance of an Electrical Double Layer. *Chem. Phys. Lett.* **2001**, *341*, 363–368.
- (14) Zhan, T.; Kumar, A.; Sevilla, M.; Sridhar, A.; Zeng, X. Temperature Effects on CO2 Electroreduction Pathways in an Imidazolium-Based Ionic Liquid on Pt Electrode. *J. Phys. Chem. C* **2020**, *124*, 26094–26105.
- (15) Ghatee, M. H.; Zare, M.; Moosavi, F.; Zolghadr, A. R. Temperature-Dependent Density and Viscosity of the Ionic Liquids 1-Alkyl-3-Methylimidazolium Iodides: Experiment and Molecular Dynamics Simulation. *J. Chem. Eng. Data* **2010**, *55*, 3084–3088.
- (16) Yang, Z.; Wullschleger, S. D.; Liang, L.; Graham, D. E.; Gu, B. Effects of Warming on the Degradation and Production of Low-Molecular-Weight Labile Organic Carbon in an Arctic Tundra Soil. *Soil Biol. Biochem.* **2016**, *95*, 202–211.
- (17) Roy Chowdhury, T.; Herndon, E. M.; Phelps, T. J.; Elias, D. A.; Gu, B.; Liang, L.; Wullschleger, S. D.; Graham, D. E. Stoichiometry and Temperature Sensitivity of Methanogenesis and CO2 Production from Saturated Polygonal Tundra in Barrow, Alaska. *Glob. Chang. Biol.* 2015, 21, 722–737.
- (18) Krupp, H.; Sperling, G. Theory of Adhesion of Small Particles. J. Appl. Phys. 1966, 37, 4176–4180.
- (19) Zaporski, J.; Yang, Z. Effects of Magnetite on Phosphorus Storage and Carbon Cycling in Lake Michigan Shoreline Sediments. *Appl. Geochem.* **2022**, *140*, No. 105293.
- (20) Uysal, A.; Zhou, H.; Feng, G.; Lee, S. S.; Li, S.; Fenter, P.; Cummings, P. T.; Fulvio, P. F.; Dai, S.; McDonough, J. K.; Gogotsi, Y. Structural Origins of Potential Dependent Hysteresis at the Electrified Graphene/Ionic Liquid Interface. *J. Phys. Chem. C* **2014**, *118*, 569–574.
- (21) Vila, J.; Fernández-Castro, B.; Rilo, E.; Carrete, J.; Domínguez-Pérez, M.; Rodríguez, J. R.; García, M.; Varela, L. M.; Cabeza, O. Liquid–Solid–Liquid Phase Transition Hysteresis Loops in the Ionic Conductivity of Ten Imidazolium-Based Ionic Liquids. *Fluid Phase Equilib.* **2012**, 320, 1–10.
- (22) Gore, T. R.; Bond, T.; Zhang, W.; Scott, R. W. J.; Burgess, I. J. Hysteresis in the Measurement of Double-Layer Capacitance at the Gold-Ionic Liquid Interface. *Electrochem. Commun.* **2010**, *12*, 1340–1343.
- (23) Drüschler, M.; Huber, B.; Passerini, S.; Roling, B. Hysteresis Effects in the Potential-Dependent Double Layer Capacitance of Room Temperature Ionic Liquids at a Polycrystalline Platinum Interface. J. Phys. Chem. C 2010, 114, 3614–3617.
- (24) Wang, Z.; Mu, X.; Guo, M.; Huang, Y.; Mason, A. J.; Zeng, X. Methane Recognition and Quantification by Differential Capacitance at the Hydrophobic Ionic Liquid-Electrified Metal Electrode Interface. *J. Electrochem. Soc.* **2013**, *160*, B83–B89.
- (25) Lin, L.; Zhao, P.; Mason, A. J.; Zeng, X. Characterization of the Ionic Liquid/Electrode Interfacial Relaxation Processes Under Potential Polarization for Ionic Liquid Amperometric Gas Sensor Method Development. ACS Sens. 2018, 3, 1126–1134.
- (26) Biskaborn, B. K.; Smith, S. L.; Noetzli, J.; Matthes, H.; Vieira, G.; Streletskiy, D. A.; Schoeneich, P.; Romanovsky, V. E.; Lewkowicz, A. G.; Abramov, A.; Allard, M.; Boike, J.; Cable, W. L.; Christiansen, H. H.; Delaloye, R.; Diekmann, B.; Drozdov, D.; Etzelmüller, B.; Grosse, G.; Guglielmin, M.; Ingeman-Nielsen, T.; Isaksen, K.; Ishikawa, M.; Johansson, M.; Johannsson, H.; Joo, A.; Kaverin, D.; Kholodov, A.; Konstantinov, P.; Kröger, T.; Lambiel, C.; Lanckman, J.-P.; Luo, D.; Malkova, G.; Meiklejohn, I.; Moskalenko, N.; Oliva, M.; Phillips, M.; Ramos, M.; Sannel, A. B. K.; Sergeev, D.; Seybold, C.; Skryabin, P.; Vasiliev, A.; Wu, Q.; Yoshikawa, K.; Zheleznyak, M.; Lantuit, H. Permafrost Is Warming at a Global Scale. *Nat. Commun.* 2019. 10. 264.
- (27) Kerlé, D.; Ludwig, R.; Geiger, A.; Paschek, D. Temperature Dependence of the Solubility of Carbon Dioxide in Imidazolium-Based Ionic Liquids. *J. Phys. Chem. B* **2009**, *113*, 12727–12735.

- (28) Kubo, R. The Fluctuation-Dissipation Theorem. Rep. Prog. Phys. 1966, 29, 255-284.
- (29) Klähn, M.; Seduraman, A. What Determines CO2 Solubility in Ionic Liquids? A Molecular Simulation Study. *J. Phys. Chem. B* **2015**, *119*, 10066–10078.
- (30) Bedrov, D.; Piquemal, J.-P.; Borodin, O.; MacKerell, A. D.; Roux, B.; Schröder, C. Molecular Dynamics Simulations of Ionic Liquids and Electrolytes Using Polarizable Force Fields. *Chem. Rev.* **2019**, *119*, 7940–7995.
- (31) Hudak, E. M.; Kumsa, D. W.; Martin, H. B.; Mortimer, J. T. Electron Transfer Processes Occurring on Platinum Neural Stimulating Electrodes: Calculated Charge-Storage Capacities Are Inaccessible during Applied Stimulation. *J. Neural Eng.* **2017**, *14*, No. 046012.
- (32) Rand, D. A. J.; Woods, R. The Rest Potential of Platinum Electrodes in Oxygensaturated 1 M Sulphuric Acid. *J. Electroanal. Chem. Interfacial Electrochem.* **1973**, 47, 353–361.
- (33) Hoare, J. P. Rest Potentials in the Platinum-Oxygen-Acid System. J. Electrochem. Soc. 1962, 109, 858.
- (34) Shibata, S. Conductance Measurement of Thin Oxide Films on a Platinum Anode. *Electrochim. Acta* 1977, 22, 175–179.

### ☐ Recommended by ACS

## Plasma-Polymerized and Iodine-Doped Polyvinyl Acetate for Volatile Organic Compound Gas Sensing Applications

Baliram Nadekar, Pravin More, et al.

FEBRUARY 28, 2023

ACS APPLIED POLYMER MATERIALS

READ 🗹

#### Exploitation of Schottky-Junction-based Sensors for Specifically Detecting ppt-Concentration Gases

Shipu Xu, Hailin Peng, et al.

DECEMBER 08, 2022

ACS SENSORS

READ 🗹

## Comprehensive Review of Fuel-Cell-Type Sensors for Gas Detection

Mehdi Mehrpooya, Ali Allahyarzadeh, et al.

FEBRUARY 06, 2023

INDUSTRIAL & ENGINEERING CHEMISTRY RESEARCH

READ

#### Nonanal Gas Sensors Using Porous Glass as a Reaction Field for Ammonia-Catalyzed Aldol Condensation

Masato Tsujiguchi, Yasuko Yamada Maruo, et al.

FEBRUARY 13, 2023

ACS OMEGA

READ 🗹

Get More Suggestions >